Model-Based Evaluation of Methods for Respiratory Sinus Arrhythmia Estimation

John Morales, Jonathan Moeyersons, Pablo Armañac, Michele Orini, Luca Faes, Sebastiaan Overeem, Merel Van Gilst, Johannes Van Dijk, Sabine Van Huffel, Raquel Bailón, and Carolina Varon

Abstract*—*Objective: **Respiratory sinus arrhythmia (RSA) refers to heart rate oscillations synchronous with respiration, and it is one of the major representations of cardiorespiratory coupling. Its strength has been suggested as a biomarker to monitor different conditions, and diseases. Some approaches have been proposed to quantify the RSA, but it is unclear which one performs best in specific scenarios. The main objective of this study is to compare seven state-of-the-art methods for RSA quantification using data generated with a model proposed to simulate, and control the RSA. These methods are also compared, and evaluated on a real-life application, for their ability to capture changes in cardiorespiratory coupling during sleep.** ***Methods:*** **A simulation model is used to create a dataset of heart rate variability, and respiratory signals with controlled RSA, which is used to compare the RSA estimation approaches. To compare the methods objectively in real-life applications, regression models trained on the simulated data are used to map the estimates to the same measurement scale.** ***Results, and conclusion:*** **RSA estimates based on cross entropy, time-frequency coherence, and subspace projections showed the best performance on simulated data. In addition, these estimates captured the expected trends in the changes in cardiorespiratory coupling during sleep similarly.** ***Significance:*** **An objective comparison of methods for RSA quantification is presented to guide future analyses. Also, the proposed simulation model can be used to compare existing, and newly proposed RSA estimates. It is freely accessible online.**

***Index Terms*—Cardiorespiratory coupling, heart rate variability, respiratory sinus arrhythmia.**

I. Introduction

THE respiratory sinus arrhythmia (RSA) is one form of cardiorespiratory coupling, characterized by an increased heart rate (HR) during inhalation and a decreased HR during exhalation. Although, two other forms of cardiorespiratory coupling have been identified [1], namely, cardiorespiratory phase synchronization and time delay stability, RSA is the most widely studied. It was initially reported in 1733, but firstly recorded in dogs only in 1847 [2]. Since then, the underlying mechanisms responsible for RSA, as well as its physiological function, have been a subject of debate.

Initially, it was thought that RSA was originated by one of two factors: either mechanical effects of respiration or the result of the regulatory action of the Autonomic Nervous System (ANS) [3]. Later studies in dogs demonstrated that both, mechanical and ANS modulations, contribute to RSA [3]. It has also been suggested that arterial baroreceptors, chemoreceptors as well as lung and heart stretch receptors play an important role in this modulation [4]–[6].

Concerning the physiological function of RSA, a widely accepted hypothesis suggests that RSA helps to match perfusion and ventilation during the respiratory cycle, thereby optimizing the oxygen uptake [7]. Nevertheless, additional tests are needed to prove this hypothesis [8]. Furthermore, other studies suggest that RSA's purpose is to either minimize the heart's workload or regulate the blood pressure. [9]–[11].

Despite the limited understanding of the mechanisms and function of RSA and the lack of a gold standard for its evaluation, it has been suggested as a biomarker to assess people's health status. For instance, RSA has been found to change with aging, diabetes, sleep apnea, heart failure, stress and anxiety disorders [12]–[17].

Manuscript received May 22, 2020; revised September 4, 2020; accepted September 23, 2020. Date of publication October 1, 2020; date of current version May 20, 2021. Funding: BOF, C24/15/036, C24/18/097. FWO. VLAIO, 150466: OSA+, O&O HBC 2016 0184 eWatch. IMEC funds 2020. EU H2020 MSCA-ITN-2018: INSPiRE-MED #813120. EU H2020 MSCA-ITN-2018: INFANS #813483. EIT Health - SeizeIT2 CIBER, Gobierno de Aragón (Reference Group BSICoS T39-20R) cofunded by FEDER 2014-2020 "Building Europe from Aragón"; and through a personal PhD grant to P.A; and Ibercaja-CAI program for research stays, code IT 9/19. HealthBed study was supported by a grant from EIT Health (project no. 18453), L.F. is supported by the Italian MIUR PRIN 2017 project, PRJ-0167, "Stochastic forecasting in complex systems" *(Corresponding author: John Morales.)*

John Morales is with the ESAT - STADIUS, Stadius Centre for Dynamical Systems, Signal Processing, and Data Analytics, KU Leuven, 3001 Leuven, Belgium and also with the KU Leuven Institute for AI, 3001 Leuven, Belgium (e-mail: jmorales@esat.kuleuven.be).

Jonathan Moeyersons and Sabine Van Huffel are with the ESAT - STADIUS, Stadius Centre for Dynamical Systems, Signal Processing, and Data Analytics and also with the KU Leuven Institute for AI.

Pablo Armañac and Raquel Bailón are with the Biomedical Signal Interpretation, and Computational Simulation (BSICoS) Group, University of Zaragoza, and CIBER-BBN.

Michele Orini is with the Institute of Cardiovascular Science, University College London, and also with Barts Heart Centre, St Bartholomews Hospital, University College London.

Luca Faes is with the Department of Engineering, University of Palermo.

Sebastiaan Overeem, Merel Van Gilst, and Johannes Van Dijk are with the Department of Electrical Engineering, Eindhoven University of Technology and also with the Sleep Medicine Center Kempenhaeghe.

Carolina Varon is with the ESAT - STADIUS, Stadius Centre for Dynamical Systems, Signal Processing, and Data Analytics as well as with the KU Leuven institute for AI, and also with the Circuits and Systems (CAS) Group, Delft University of Technology.

Digital Object Identifier 10.1109/TBME.2020.3028204

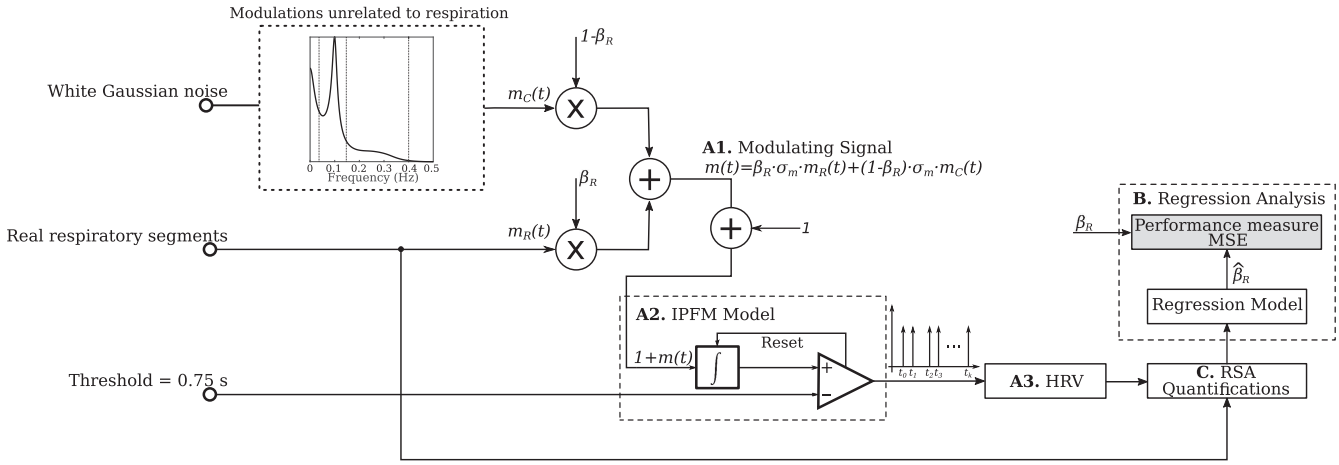

Fig. 1. Model for the simulation study. The numerals correspond to the section in the paper where each part is described. A1. $m(t)$ represents the action of different modulators in the SA node. The RSA strength is modeled by β_R. A2. $m(t)$ is used to produce a train of impulses representing the heart beats generation. A3. A HRV representation is calculated using this train of impulses. C. The HRV and respiratory signals are used to estimate the RSA strength with different methods. B. Regression models are built to predict β_R with the different RSA estimates. This prediction results in an mean squared error.

The debate over RSA's function and its potential use as biomarker in different conditions demonstrates the importance of standardizing methods for RSA assessment. A common approach to evaluate RSA in a non-invasive way is through heart rate variability (HRV). HRV captures the variation of inter-beat intervals that occurs due to modulations from the ANS. HRV can be computed by first detecting the R-peaks in the Electrocardiogram (ECG) signal. From the R-peak locations, different HRV representations can be used, including the interval tachogram, the inverse interval tachogram, the interval function, the inverse interval function and the heart timing signal [18]. A common approach to evaluate RSA using HRV is to calculate its power spectrum and then compute the total power in the High Frequency (HF, 0.15-0.4 Hz) band [19], assuming that respiratory frequency ranges between 9 and 24 breaths per minute. However, respiration might occur in frequencies outside this range and misleading results might be obtained using this estimation [20]–[23].

Alternative approaches to estimate RSA that do not consider specific frequency bands have been suggested in literature, including the use of respiratory bandwidths [24], [25], time frequency (TF) decompositions [26], [27], subspace projections [16], bivariate phase rectified signal averaging (BPRSA) [28], entropy calculations [29] and pole specific spectral causality (PSSC) [30]. Currently, it is unclear which of these approaches is more appropriate to estimate RSA and under which conditions.

The goal of this study is to perform a detailed comparison of the aforementioned approaches. To achieve this, a model to evaluate different RSA estimation methods is proposed. Some models exist in literature, such as the ones presented in [9], [31], [25], [32], [33]. However, these do not allow to modify the RSA strength, are not available on-line, and do not always use real respiratory signals. This paper introduces a new model that allows to control the RSA, use real respirations with different spectral characteristics and is available to be downloaded.

Seven RSA estimates are evaluated and applied to simulated as well as to data recorded during full-night polysomnography of healthy volunteers. Here, scenarios where the coupling strength is different (e.g., REM vs. NREM sleep), are used to evaluate RSA estimates in real data [34], [35].

II. Methodology

A. Simulation Model

The model used in the simulation is shown in Fig. 1. Important aspects and components of the model are:[1]

1) Datasets Used in the Simulation: Signals from 3 datasets were used to built and parametrize the simulation. The first one contains thoracic respirations and lead V1 ECG signals (Sampling frequency, $F_s = 500$ Hz) from 110 patients with different severities of obstructive sleep apnea and associated comorbidities [24]. Here, segments containing apneas were removed based on the annotations given by the specialists using the AASM 2012 scoring rules [36]. It is important to mention that the cardiorespiratory coupling is affected in apnea patients, even during apnea-free periods [24]. However, in the simulation only the respiratory signals are used. The second dataset consists of thoracic respiratory ($F_s = 31$ Hz) and lead II ECG signals ($Fs = 486$ Hz) taken from the stress recognition in the automobile drivers' dataset available in Physionet. This dataset was recorded from 16 healthy volunteers while driving a car around Boston, Massachusetts [37]. The third one is the Fantasia dataset, also from Physionet, which contains ECG and thoracic respiratory effort signals ($F_s = 250$ Hz) collected from 40 healthy volunteers

[1]The implementation of the model is available in: https://gitlab.esat.kuleuven.be/biomed-public/rsa-simulation-model

TABLE I
MODIFIED COEFFICIENTS AND STANDARD DEVIATION OF THE AR MODEL USED IN THE SIMULATION TO GENERATE m_C. THESE ARE CALCULATED WITH SIGNALS AT A SAMPLING RATE OF 1 HZ

a_0	a_1	a_2	a_3	a_4	a_5	a_6	a_7	σ_m^2
1	-1.8149	1.7048	-1.3868	1.1625	-0.6484	0.2602	-0.1598	$6.7 \cdot 10^{-3}$

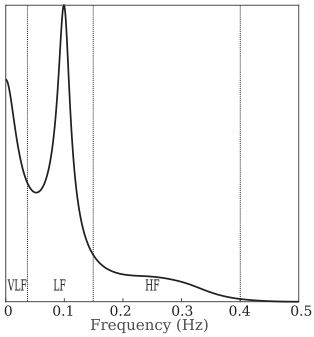

Fig. 2. Frequency response of the filter based on the AR coefficients reported in [39]. This filter is used to generate m_C with an attenuated HF component.

at rest, while watching the movie Fantasia (Disney, 1940) [38]. The reason to use three datasets is to consider respirations with distinct spectral characteristics.

The respiratory signals were filtered to preserve frequency components between 0.03 and 0.9 Hz, upsampled to 1000 Hz and then cut into 5-minutes epochs. These were visually inspected and those severely contaminated with artifacts were removed. The remaining ones were divided, based on their power spectrum, into two groups. The first one, referred to as regular, was composed of the respiratory signals with power contained inside the HF band. The second one, referred to as irregular, comprised the signals with a spectrum broader than or outside the HF band. In order to balance the contribution of each dataset in the simulation, a maximum of 300 randomly selected 5-minutes epochs, per dataset, were used.

2) Modulating Signal $\mathbf{m(t)}$***:*** The signal $m(t)$ models the mechanisms modulating the electrical activity of the sinoatrial node. It is built by adding two components. The first one represents the HRV changes correlated with respiration ($m_R(t)$). This component was derived randomly taking a respiratory 5-minutes segment. The second is its complement and models the modulations not correlated with respiration ($m_C(t)$). To generate it, a filter was built based on the autoregressive (AR) model described in [39], which assumes a sampling rate of 1 Hz. In the current work, these coefficients were modified to remove the peak in the HF band which, in healthy subjects during controlled breathing, is mainly due to respiration [40]–[42]. The modified AR coefficients are given in Table I. The frequency response of the filter is shown in Fig. 2. A 5-minutes white Gaussian noise epoch with $F_s = 1$ Hz and unit variance was generated and then filtered with the aforementioned filter to obtain the modulation not correlated with respiration. The resulting signal was then upsampled to 1000 Hz and constitutes $m_c(t)$.

Next, $m_R(t)$ and $m_C(t)$ were normalized to have zero mean and unitary standard deviation. These were used to build $m(t)$ as,

$$m(t) = \beta_R \cdot \sigma_m \cdot m_R(t) + (1 - \beta_R) \cdot \sigma_m \cdot m_C(t), \quad (1)$$

where σ_m is the standard deviation of the modulating signal. The coefficient β_R models the strength of the cardiorespiratory coupling, where $0 \leq \beta_R \leq 1$. In order to select σ_m^2, the ECG recordings from the Fantasia and drivers datasets were used. These two datasets were included so that only healthy subjects were considered. From these ECG recordings, the R-peaks were detected using the algorithm described in [43]. Next, the modulating signals were estimated using the IPFM model [39]. Afterwards, these modulating signals were segmented into 5-minutes epochs and their variances were calculated. As a result, σ_m^2 was defined as the mean variance of all the epochs.

3) Integral Pulse Frequency Modulation (IPFM) Model: The IPFM model is described in [18], [44] and is based on the idea that $m(t)$ represents the action of the different mechanisms that modulate the SA node. When the integral of $1 + m(t)$ reaches a threshold T, an impulse is generated. T represents the mean heart period and constitutes the intrinsic sampling rate of the heart rate variability [39]. In this study, it is fixed to 0.75 s, corresponding to a mean HR of 90 beats per minute. This value was obtained after analyzing the spectral characteristics of the respiratory segments described in Section II-A1. The upper limit of the 95% occupied bandwidth was calculated on each segment. The 90$^{\text{th}}$ percentile of this upper limit was 0.74 Hz. A sampling rate of 1.48 Hz would be required to sample these signals without aliasing, corresponding to a mean HR of 89.56 BPM and a mean heart period of 0.74 s.

After selecting the simulation model parameters, it was used to generate a train of impulses representing the beat occurrence time series modulated by $m(t)$.

4) HRV Representations: The inverse interval function, $d_{IIF}(t)$, was computed from the inverse of the RR interval series derived from the beat occurrence time series. This was shown to outperform other HRV representations to capture modulating signal information [18]. The result was interpolated to a uniform sampling frequency, resulting in $d_{IIF}(n)$, and then used to compute the RSA estimates explained later in Section II-C.

B. Model Application

The simulation model was used for assessing the capability of each RSA estimate to predict β_R, which was evaluated using regression models. To this end, the simulation was run 50 times while varying β_R in the interval [0.02 1] in steps of 0.02, randomly choosing a respiratory segment each time, ensuring that the amount of used regular and irregular respiratory segments was balanced. This, in turn, was repeated 100 times to build a dataset of RSA estimates with known β_R. This dataset was

then randomly split into a training set comprising 80% of the samples, and a test set with the remaining 20%.

Afterwards, support vector machines (SVM) regression models with radial basis function kernels were built on the training set using each of the RSA estimates independently. The hyperparameters were tuned using grid search with 10-fold cross-validation in the training set. After training the regression model, β_R was predicted on the test set. This prediction is denoted $\hat{\beta}_R$. To compare the methods, the mean squared error (MSE) in the test set was used as performance metric, calculated as,

$$MSE = \frac{1}{I}\sum_{i=1}^{I}\left(\beta_{R_i} - \widehat{\beta}_{R_i}\right)^2, \tag{2}$$

where I is the total number of samples in the test set.

To statistically compare the MSE of each RSA estimate, this procedure was repeated 100 times, where the training and test sets were selected at random.

For comparison purposes, the simulation was repeated in the following scenarios:

- Separating regular and irregular respiratory segments. This was done to evaluate the effect of having respirations with different spectral characteristics. A sampling rate of 4 Hz was used for the HRV and respiratory signals.
- Using two sampling frequencies (2 and 4 Hz) for the HRV and respiration. The reason to use two sampling frequencies is to evaluate the relationship between this parameter and the performance of the RSA estimates. On the one hand, 4 Hz was included since it is widely used in applications where a high HR is expected, such as during exercise. On the other hand, 2 Hz was used to study the effect of a lower sampling rate.

C. RSA Estimates

At this point, the respiratory signals were resampled to the same sampling frequency as the HRV. The evenly-sampled respiratory signals ($x_1(n)$) and HRV ($x_2(n)$) were used to estimate the cardiorespiratory coupling with 7 different approaches, which are classified into two categories:

1) Model-Free Approaches: This category groups non-parametric methods, including spectral analysis, BPRSA curves and a TF representation.

a) Normalized HRV power in the extended HF band: The PSD of the HRV was calculated with the Welch periodogram and a hamming window of 40 seconds with 50% overlap. Commonly, the spectrum of the HRV is divided into three frequency intervals, namely very low frequency (VLF, 0.003-0.04 Hz), low frequency (LF, 0.04-0.15 Hz) and high frequency (HF, 0.15-0.4 Hz) [19].The LF band contains information about sympathetic and vagal modulations. The HF band is related to vagal and respiratory activities. In this work, the lower limit of the HF band was defined as 0.15 Hz. The upper limit was extended to the maximum between 0.4 Hz and half the mean HR. This modification was done to account for cases in which the respiratory rate goes above 0.4 Hz. According to previous studies, respiratory rates above the HF band might be commonly observed during daily activities or exercise [26]. The power

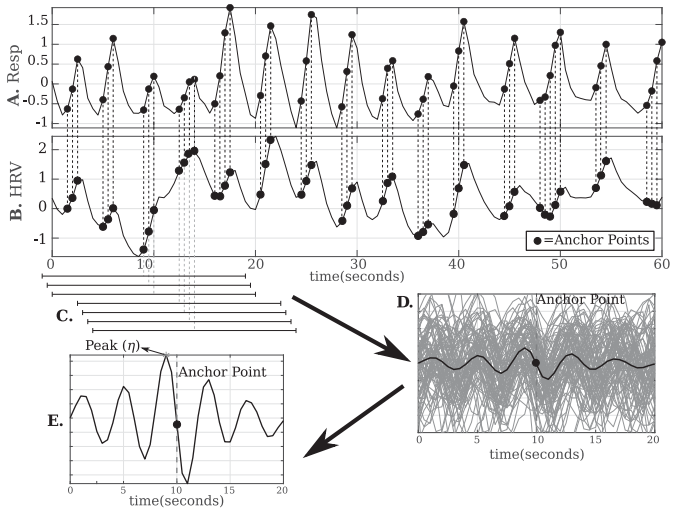

Fig. 3. Estimation of the RSA using the BPRSA curves. A: Respiration (driver signal) in which AP's (•) are defined. B: HRV representation. The AP's defined in the respiration are used to extract signal portions from the HRV. C: These portions are extracted. D: The segments (gray) are averaged to obtain the PRSA curve (black). E: Resulting PRSA curve and feature.

contained in the extended HF band was calculated and normalized by the total power in the band between 0.04 Hz and the upper limit of the extended HF band. This parameter is referred to as P_{HF}.

b) Normalized HRV power in the respiratory bandwidth: The PSD of the respiration was calculated with the Welch periodogram and a hamming window of 40 seconds with 50% overlap. It was then used to define the frequency band in the HRV that contained the breathing information. For this, the -3 dB bandwidth relative to the main peak of the respiratory signal was identified. Next, the influence of the respiration on HRV was quantified as the normalized power contained in the PSD of the HRV in the same band. The normalization was done with respect to the band between 0.04 Hz and the upper limit of the extended HF band. This estimation is denoted P_{BW} [24].

c) Maximum of the BPRSA curve: The calculation of the BPRSA curves is illustrated in Fig. 3. These curves capture quasi periodicities in a target signal (HRV) caused by changes in a driver signal (respiration). In this paper, the derivation of the BPRSA curves was done by first locating the upslope points in the respiration [45]. These are known as anchor points (AP). Afterwards, segments of the HRV were defined in windows of 20 seconds centered around the APs. Next, these epochs were averaged to obtain the BPRSA curves. The curve's peak value (η) was calculated and evaluated as RSA estimate.

d) Average normalized power of the partial spectrum of the HRV related to respiration: This approach is based on the model in Fig. 4. Here, $x_2(n)$, denoting the HRV, is modeled as the contribution of two components. The first one due to the respiration ($x_{2_R}(n)$) and the second one due to other modulators ($x_{2_C}(n)$). As shown in [46], the TF spectrum of $x_2(n)$ can be decomposed into the partial spectra of $x_{2_R}(n)$ and $x_{2_C}(n)$ based on the TF coherence between HRV ($x_2(n)$) and respiration ($x_1(n)$). To this

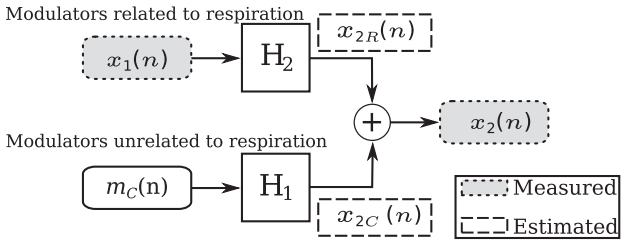

Fig. 4. Model of the different modulators in the HRV using a two-input, one-output representation as described in [46].

end, the TF spectra of $x_1(n)$ and $x_2(n)$ were calculated using the Cohen's Class Distribution proposed in [27]. Secondly, the TF coherence (γ) between $x_1(n)$ and $x_2(n)$ was derived. Next, the partial spectrum of $x_{2_R}(n)$ was estimated as the product between γ^2 and the spectrum of $x_2(n)$ [27]. Afterwards, the instantaneous power of $x_{2_R}(n)$ was obtained integrating its partial spectrum in the band between 0.04 Hz and the upper limit of the extended HF band. Finally, this result was normalized by the instantaneous power of $x_2(n)$ in the same band and then averaged over time to obtain an estimate of the RSA, denoted P_{TF}.

2) Model Based Approaches: The approaches included in this category are based on or explained with multivariate autoregressive (MVAR) models. To build these models, a time-varying vector $\boldsymbol{x}(n) = [x_1(n)\ \ x_2(n)]^T$ is constructed, where $x_1(n)$ and $x_2(n)$ represent the respiration and HRV signals, respectively. The interactions between both systems are modeled as,

$$\boldsymbol{x}(n) = \sum_{k=1}^{L} \boldsymbol{A}(k)\boldsymbol{x}(n-k) + \boldsymbol{w}(n), \tag{3}$$

where $\boldsymbol{w}(n) = [w_1(n)\ \ w_2(n)]^T$ represents two independent residual noise signals, and L is the model order. The term $\boldsymbol{A}(k)$ denotes a 2×2 matrix, defined as,

$$\boldsymbol{A}(k) = \begin{bmatrix} \boldsymbol{a}_{11}(k) & \boldsymbol{a}_{12}(k) \\ \boldsymbol{a}_{21}(k) & \boldsymbol{a}_{22}(k) \end{bmatrix}, \tag{4}$$

representing the interactions between the HRV and respiration. Here, $\boldsymbol{a}_{ij}(k)$ are the coefficients representing the influence of the i^{th} system on the j^{th} system. The methods to estimate RSA included in this category differ in the way they solved for $\boldsymbol{A}(k)$ or interpret the model.

The order L might influence the results significantly. Its selection was first tested with the Akaike's information criterion (AIC) and minimum description length (MDL). However, the results were not always consistent being usually too different with the two methods. For this reason, the model order was chosen with a more empirical approach. First, a frequency (F_r) representative of the respiratory dynamics was found. For this, the PSD of the respiration was computed as described in Section II-C1. Next, the band containing the 90% of the total power was calculated. Afterwards, the $\mathcal{M}$ modes (i.e. local maxima) inside this band were found and put in a set $\boldsymbol{D} = (F_{mi}, P_{mi})_{mi=1}^{\mathcal{M}}$, containing the F_{mi} frequencies of the modes and their P_{mi} powers. If $\mathcal{M} \leq 3$, F_r was defined as the F_{mi} such that its associated P_{mi} was the maximum. In case that $\mathcal{M} > 3$, $F_r = min(F_{mi})$, but if $F_r < 0.1$ Hz, it was fixed to 0.1. The order L was calculated as the number of samples required to capture two periods of F_r. This approach is depicted in Algorithm 1.

Algorithm 1: Selection of Model Order for AR Models.

Result: Model order L
1. Compute PSD of respiration;
2. Find 90% bandwidth (OBW);
3. Find number of modes inside OBW ($\mathcal{M}$);
4. Define $D = (F_{mi}, P_{mi})_{mi=1}^{\mathcal{M}}$;
5. **if** $\mathcal{M} \leq 3$ **then**
   $F_r = F_{mi}$ s.t. $max(P_{mi})$;
   else
   $F_r = min(F_{mi})$;
   end
   if $F_r < 0.1$ Hz **then**
   $F_r = 0.1$ Hz;
   end
6. Calculate the model order as $L = \dfrac{2F_s}{F_r}$

a) Cross Entropy: The cross entropy (CE) measures the information in the present sample of the HRV resolved by the past of the respiration. To compute the CE, the model in equation 3 was solved for $\boldsymbol{A}(k)$ using the autocovariance method [47]. In the resulting $\boldsymbol{A}(k)$, the entry $\boldsymbol{a}_{ij}(k)$ describes the coefficients of a regression, predicting $x_j(n)$ in function of $x_i(n-k)$, with $i, j = 1, 2$. The variance of the HRV ($\sigma^2(x_2(n))$) as well as the variance of the residuals of the regression between the present samples of the HRV and the past information of the respiration ($\sigma^2(x_2(n) \mid x_1^-(n))$) were calculated as described in [31]. The cross entropy was then derived as,

$$CE = \frac{1}{2} \ln \frac{\sigma^2(x_2(n))}{\sigma^2(x_1(n) \mid x_2^-(n))}. \tag{5}$$

The cross-entropy in equation 5 was estimated with a linear approach since the data is assumed to follow a Gaussian distribution [48].

b) Proportion of variance related to respiration given by Pole Specific Spectral Causality (PSSC): This approach quantified the interactions between the respiration and HRV in the frequency domain in specific bands [30]. For this, the Z-transform was applied to the system in equation (3) to obtain $\boldsymbol{x}(z) = \boldsymbol{H}(z)\boldsymbol{w}(z)$, where,

$$\boldsymbol{H}(z) = \begin{bmatrix} H_{11}(z) & H_{12}(z) \\ H_{21}(z) & H_{22}(z) \end{bmatrix} = [\mathbf{I} - \mathbf{A}(z)]^{-1} \tag{6}$$

and

$$\mathbf{A}(z) = \sum_{k=1}^{L} \mathbf{A}(k) z^{-k}, \tag{7}$$

is the matrix $\boldsymbol{A}(k)$ in the Z domain. $\mathbf{H}(z)$ is known as the transfer matrix and it is the frequency domain representation of the dynamic dependencies within and between the HRV and respiratory signals. The terms $H_{ij}(z)$ can be understood as

transfer functions characterizing the relationship between the i^{th} and the j^{th} systems. The power spectrum of system i, $i = 1, 2$, can be decomposed into two partial spectra. The first spectrum is related to the dynamics of the system itself and described by the transfer function $H_{ii}(z)$. The second one is related to the dynamics of the other system and described by the transfer function $H_{ij}(z)$. From these, the complex partial spectra can be obtained as,

$$S_{x_{i|j}}(z) = \sigma^2_{w_j} H_{ij}(z) H_{ij}(z^{-1}), \tag{8}$$

where $\sigma^2_{w_j}$ is the variance of the j^{th} process. In [30], it was shown that each partial spectrum can be expanded to L components related to the poles of the transfer function as,

$$S_{x_{i|j}}(z) = \sum_{k=1}^{L} S^{(k)}_{x_{i|j}}(z). \tag{9}$$

These terms are integrated in the whole frequency range, given by the sampling frequency F_s, allowing to decompose the variance of the i^{th} process as,

$$\begin{aligned}\sigma^2_{x_i} &= \sum_{k=1}^{L} \int_0^{\frac{F_s}{2}} S^{(k)}_{x_{i|i}}(f)\, df + \sum_{k=1}^{L} \int_0^{\frac{F_s}{2}} S^{(k)}_{x_{i|j}}(f)\, df \\ &= \sum_{k=1}^{L} p_i(k) = \sum_{k=1}^{L} (p_{i|i}(k) + p_{i|j}(k)),\end{aligned} \tag{10}$$

where,

$$p_{i|j}(k) = \sum_{k=1}^{L} \int_0^{\frac{F_s}{2}} S^{(k)}_{x_{i|j}}(f)\, df. \tag{11}$$

Here, $p_{i|i}(k)$ is the part of the variance of x_i due to its own dynamics in the k^{th} oscillation. $p_{i|j}(k)$ is the part of the variance of x_i due to its interaction with x_j in the k^{th} oscillation.

Following these equations, the variances of the HRV and respiratory signals were decomposed as follows,

$$\sigma^2_{x_1} = \sum_{k=1}^{L} p_1(k) = \sum_{k=1}^{L} (p_{1|1}(k) + p_{1|2}(k)) \tag{12}$$

$$\sigma^2_{x_2} = \sum_{k=1}^{L} p_2(k) = \sum_{k=1}^{L} (p_{2|1}(k) + p_{2|2}(k)), \tag{13}$$

with $k = 1, \ldots, L$. The terms in these expressions can be interpreted as follows,

- $p_1(k)$ is the variance of the respiration captured by the k^{th} pole.
- $p_2(k)$ is the variance of the HRV captured by the k^{th} pole.
- $p_{1|1}(k)$ is the variance of the respiration explained by its own dynamics captured by the k^{th} pole.
- $p_{1|2}(k)$ is the variance of the respiration explained by the HRV and captured by the k^{th} pole.
- $p_{2|2}(k)$ is the variance of the HRV explained by its own dynamics captured by the k^{th} pole.
- $p_{2|1}(k)$ is the variance of the HRV explained by the respiration and captured by the k^{th} pole.

The Q poles in p_1, containing a variance equal or higher than 20% of the variance of the largest pole, were selected. Then, the estimation of the RSA, referred to as δ_T, was given by,

$$\delta_T = \frac{\sum_{k_m=1}^{Q} p_{2|1}(k_m)}{\sum_{k=1}^{L} p_2(k)}. \tag{14}$$

c) Normalized power of HRV linearly related to respiration: This approach decomposes the HRV into two components, one linearly related to respiration and another with residual information, using orthogonal subspace projections. For this, a subspace spanned by $\boldsymbol{V} \in \mathbb{R}^{(\mathrm{N-L+1})\times \mathrm{L}}$ was built as a time-delay embedding of the respiration using L delays [16], with N the amount of samples in the respiratory signal. $\boldsymbol{V}$ was then used to calculate a projection matrix $\boldsymbol{P} \in \mathbb{R}^{(\mathrm{N-L+1})\times(\mathrm{N-L+1})}$, given by,

$$\boldsymbol{P} = \boldsymbol{V}(\boldsymbol{V}^T\boldsymbol{V})^{-1}\boldsymbol{V}^T, \tag{15}$$

which in turn was used to derive the information in the HRV linearly correlated to the respirations,

$$\hat{\boldsymbol{x}}_{2_R} = \boldsymbol{P}\hat{\boldsymbol{x}}_2, \tag{16}$$

in which $\hat{\boldsymbol{x}}_2 = [x_2(1), x_2(2), \ldots, x_2(N-L+1)]$. This decomposition can be understood from the MAR model in equation 3. Subspace projections can be seen as a different approach to calculate $\boldsymbol{a}_{21}(k)$ using the past information of the respiration and the present samples of the HRV.

Within this approach, RSA is estimated as the relative power of the linear respiratory influences on the HRV, computed as,

$$\mathcal{P}_x = (\hat{\boldsymbol{x}}^T_{2_R}\hat{\boldsymbol{x}}_{2_R})/(\hat{\boldsymbol{x}}^T_2\hat{\boldsymbol{x}}_2). \tag{17}$$

D. Application to Real Data

In order to test the algorithms on real data, the RSA estimates were derived from full-night polysomnography signals of 84 healthy volunteers. The dataset was recorded in the Kempenhaeghe Center for Sleep Medicine in Heeze, the Netherlands. The study was approved by the Kempenhaeghe ethical committee and by the medical ethical committee of the Maxima Medical Center Eindhoven (W17.128). The ECG signals were recorded with $F_s = 512$ Hz and the respiration with $F_s = 128$ Hz. The R-peaks were detected with the approach described in [43]. Then, the inverse interval function was used as the HRV representation.

Afterwards, the HRV representations and the respiratory signals were preprocessed following the same steps as in the simulated dataset. Then, these were segmented into non-overlapping epochs of 5 minutes, and the RSA estimates were calculated using for each one the sampling frequency that showed the best performance in the simulation study. RSA estimates per subject were obtained averaging the RSA estimates on each 5-minute epoch per sleep stage and subject. These were then used to analyze the RSA during sleep stages. Changes in the RSA strength were expected since its regulation differs during wake, NREM, and REM sleep [34], [35]. The sleep stages were annotated by a technician following the AASM 2012 scoring rules.

Each of the estimates included in this paper measures RSA with a different unit and scale. For instance, one of them uses

TABLE II
SUMMARY OF THE RSA ESTIMATES COMPARED IN THIS PAPER

Feature	Description
P_{HF}	Normalized HRV power in the extended HF band
P_{BW}	Normalized HRV power in the respiratory bandwidth
η	Maximum of the BPRSA curve
P_{TF}	Average normalized power of the partial spectrum of the HRV related to respiration
CE	Cross Entropy
$\mathcal{P}_x$	Normalized power of HRV linearly related to respiration
δ_T	Proportion of variance related to respiration given by (PSSC)

s^{-1} and some other estimates are given as ratios. This makes it difficult to do an objective comparison. This problem is solved after applying the regression models derived in the simulation study, since all estimates are transformed into the same unit and scale, given by $\hat{\beta}_R$. To this end, one of the 100 models trained as explained in Section II-B was chosen for each RSA estimate. These models were then used to predict $\hat{\beta}_R$ using the RSA estimates calculated in the sleep data.

E. Execution Times

The algorithms with best performance were also compared in terms of their computational cost. For this, 1000 signals randomly selected from the simulation study were chosen, and the times to compute the different RSA estimates were measured. This was done using a 64-bits machine with an Intel core i7-7820HQ 2.9 GHz.

F. Statistical Tests

Significant differences between the parameters calculated under different conditions and significant differences between the execution times were tested using Kruskal-Wallis tests ($p < 0.05$). Significant changes on the parameters between sleep stages in the application in real data were tested using the Friedman's tests for repeated measures ($p < 0.05$). The test used in each case is mentioned in the figures. The p-values are marked in the figures as follows: a $p < 0.05$ is shown with a asterisk (*), a $p < 0.01$ is marked with two asterisks (**) and a $p < 0.001$ is illustrated with three asterisks (***).

III. RESULTS

Table II presents a summary of the RSA estimates compared in this paper.

A. Comparison of the RSA Estimates

Fig. 5 depicts 4 examples of signals in the simulation study. The corresponding RSA estimates on each case are shown in the last row of the same figure. From these examples, different aspects can be noted.

- P_{HF} resulted in consistent RSA estimates when $\beta_R = 0.3$. However, this occurs because the power content in the HF was minimal and the respiratory modulation was weak.
- P_{BW} failed to capture the RSA when the bandwidth of the respiration was wide or it overlapped with the peak in the LF band.
- η was consistent in the given examples but, as will be shown later, its performance was actually affected by respiratory signals with different spectral characteristics.
- δ_T did not produce consistent results with signals sampled at 4 Hz, but it improved when $F_s = 2$ Hz was used instead.
- P_{TF}, CE and $\mathcal{P}_x$ were the most robust approaches to respiratory signals with different spectral characteristics.

Fig. 6 shows the MSE for each RSA using $F_s = 4$ Hz and separating the analyses by the type of respiratory segment: regular or irregular. As expected, P_{BW} and P_{HF} failed to characterize β_R with the irregular respiratory segments. δ_T and η were also affected but not as much as P_{HF} or P_{BW}. For δ_T, an irregular respiration made the selection of L more challenging. The MSE probability distribution for P_{TF} was significantly affected by different types of respiration, but the median values were small in both cases. CE and $\mathcal{P}_x$ were the most robust ones to respiratory segments with different spectral characteristics. In addition, the tests with different F_s showed that model free approaches, except P_{TF}, were more robust to F_s. δ_T was significantly affected by a higher F_s. Fig. 6 and the results changing F_s show that alternative RSA estimates, except P_{BW}, produce better regressions than those based on the Welch periodogram. As an example, P_{BW} and P_{HF} produced estimates with a median MSE > 0.02 when an irregular respiration is considered. $\mathcal{P}_x$, which was the parameter that best predicted β_R, had a median MSE ≈ 0.002 when $F_s = 4$ Hz.

Fig. 7 depicts the RSA estimates in function of β_R. The plots were made using the sampling frequencies with the lowest median MSE for each estimate (2 Hz for δ_T and 4 Hz for the others). P_{BW} performed the worst of all methods, therefore, it is not included in the figure. The first plot, shows that P_{HF} did not change with β_R as consistently as the other RSA estimates, in particular when β_R increased. η showed a similar trend to P_{HF} displaying a higher variability with a stronger coupling. δ_T, P_{TF}, CE and $\mathcal{P}_x$ captured the coupling strength better than P_{HF} but each of them correlated differently to β_R. For instance, CE had an increased trend while $\mathcal{P}_x$, P_{TF} and δ_T seemed to reach a saturation point. Also, P_{TF}, $\mathcal{P}_x$ and CE were more linearly correlated with β_R compared to the other estimates. The regression models trained with the same training set were used

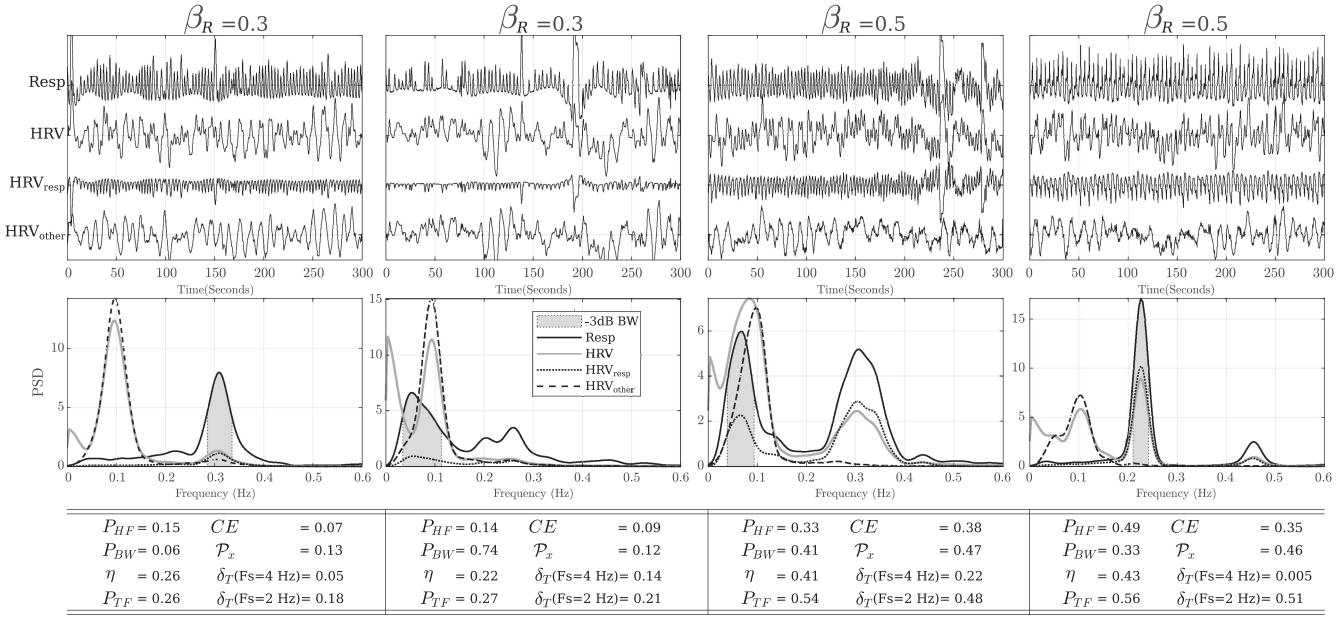

Fig. 5. Examples of signals in the simulation study with different respiratory signals and β_R. Top row: Signals and HRV decomposition with subspace projections. Middle row: PSD estimates of the signals. The gray region corresponds to the -3 dB bandwidth of the respiration. Bottom row: RSA strength estimated with the approaches included in this paper. Two examples with $\beta_R = 0.3$ and two examples with $\beta_R = 0.5$ are illustrated to show the response of the RSA estimates to respirations with different spectral characteristics but with modulating signals with the same β_R.

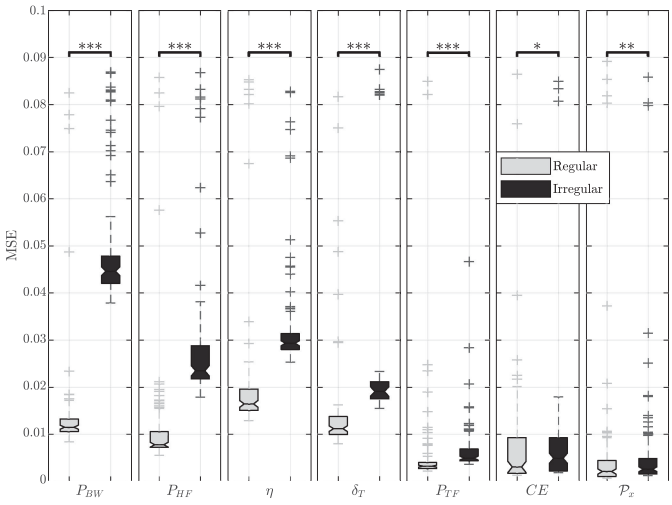

Fig. 6. MSE calculated with equation 2 in the simulation study. The results are shown for regular and irregular respiratory segments. Significant differences were tested with Kruskal-Wallis tests.

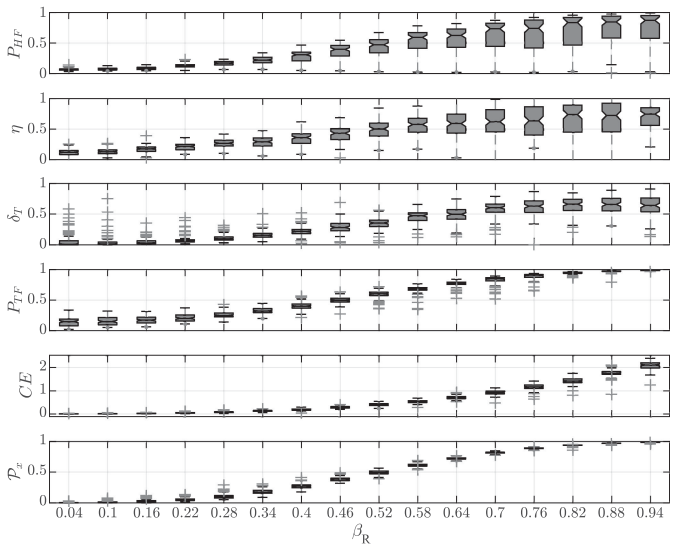

Fig. 7. Change of the RSA estimates in function of the RSA strength. The increase in the cardiopulmonary coupling is modeled with β_R.

to predict $\hat{\beta}_R$ as function of each RSA estimate.[2] The resulting prediction functions for each model are shown in Fig. 8. With these regressions, it was possible to estimate the real percentage of change in the strength of the cardiorespiratory coupling with the different RSA estimates as characterized by $\hat{\beta}_R$. In addition, a more objective comparison between the different estimates could be done, since they were transformed to the same measurement scale. The figure illustrates that CE and $\mathcal{P}_x$ changed more monotonically with β_R compared to the other estimates. Furthermore, P_{HF} and δ_T had non monotonic curves.

[2]The trained regression models in MATLAB can be found in: https://gitlab.esat.kuleuven.be/biomed-public/rsa-simulation-model

B. Application to Real Data

Fig. 9 illustrates the RSA estimates calculated in the sleep dataset. Here, δ_T was calculated with $F_s = 2$ Hz and the other

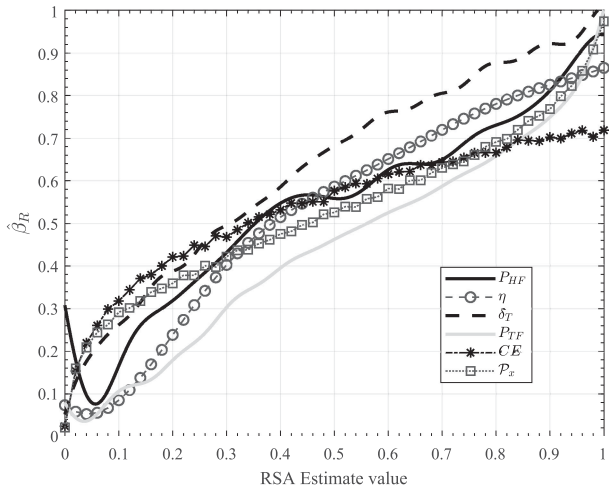

Fig. 8. Regression curves for the different RSA estimates to the equivalent β_R.

TABLE III
AMOUNT OF SEGMENTS PER SLEEP STAGE

Sleep Stage	Total	Per subject
REM & Wake	2363	28±7
NREM 1	575	7±5
NREM 2	3516	42±9
NREM 3	1625	19±7

estimates with 4 Hz. The amount of segments available per sleep stage are summarized in Table III. Note that P_{HF} quantified higher values compared to $\mathcal{P}_x$. P_{TF}, CE, δ_T and $\mathcal{P}_x$ found the same significant differences and these were similar to the ones reported in [35]. The top row shows the RSA estimates before applying the regression models. Here, it is important to mention that each RSA estimate is in a different measurement scale. $\mathcal{P}_x$, P_{HF}, δ_T and P_{TF} are in the interval [0, 1], since these are given as ratios. On the other hand, CE and η are in the interval [0 ∞]. The bottom row depicts the estimated $\hat{\beta}_R$ using the regression models derived from the simulation study. As a result, all RSA estimates are on the same measurement scale, determined by $\hat{\beta}_R$, in the interval [0 1]. The same significant differences were found in the top and bottom rows. The $\hat{\beta}_R$ calculated with CE and $\mathcal{P}_x$ were not significantly different. When comparing the $\hat{\beta}_R$ with these two RSA estimates to the ones obtained with δ_T and P_{TF}, it is observed that the median $\hat{\beta}_R$ differed by less than 0.1. More importantly, the trends with these estimates captured similarly the change in $\hat{\beta}_R$ when comparing NREM3 and wake as well as NREM2 and wake. Here, the changes in the median $\hat{\beta}_R$ were close to 0.15 and 0.06, respectively.

C. Execution Times

Fig. 10 shows the boxplots for the execution times of the 1000 random signals taken from the simulation. $\mathcal{P}_x$ and CE are faster to compute since they need simpler multiplications between matrices to be calculated. P_{TF}, on the other hand, requires the derivation of the power spectral density of the signals using the Cohen's Class distribution, which is a computationally expensive operation.

IV. DISCUSSION

A. Comparison of the RSA Estimates

Estimates based on frequency bands in the Welch periodogram displayed a lower performance because the modulations due to respiratory segments with frequency content in bands below the HF band were not captured correctly. This has been reported before [16], [24], [49] and illustrates the disadvantage of considering specific frequency bands when estimating the RSA. P_{BW} was previously reported to be better compared to P_{HF} in a dataset of patients with sleep apnea [24]. This difference compared to the results reported in the current work can be explained by the fact that in [24], only clean respiratory signals with a narrow band were considered. P_{BW} fails to successfully capture the RSA when the respiratory spectrum has a broad bandwidth or when it overlaps with the peak in the LF band. This approach might be useful in cases in which the respiratory rate falls outside the HF band under the condition that a clear spectral peak is present. CE, P_{TF} and $\mathcal{P}_x$ presented the smallest errors among the compared approaches and these were independent of the frequency distribution or sampling frequency of the respiration and HRV signals.

Regression models were used to estimate the respiratory modulation, β_R, as function of each RSA estimate. This allowed to estimate the real percentage of change in the RSA. Different aspects of the results shown in Fig. 8 should be highlighted. First, it is observed that the regression line for P_{HF} does not change monotonically with β_R. The reason for this is the variability of the estimation, in particular when β_R is large, affecting the training of the regression model. In addition, $\mathcal{P}_x$ and CE have a more linear behavior. In the case of $\mathcal{P}_x$, this linearity holds in the interval $0.2 < \beta_R < 0.7$. For CE, the linear relationship is maintained in the whole interval, and holds up to $\beta_R = 0.95$. P_{TF} and η display a more monotonic behavior compared to P_{HF}. In general, the results suggest that the estimates with a more linear relationship with β_R have a better performance.

An important comparison is between P_{HF} and $\mathcal{P}_x$, since they can be considered to estimate the RSA in a similar way as a percentage of power in the HRV explained by respiration. These estimates have been compared in previous works [16], [49]. The results of the simulation indicate that, depending on the weight of the respiratory modulation with respect to other modulations, P_{HF} results in an underestimation or overestimation of the power explained by respiration in the HRV compared with $\mathcal{P}_x$, as displayed in Fig. 7. When the weight of the respiratory modulation is higher ($\beta_R > 0.5$) than the weight of other modulators, P_{HF} is more likely to underestimate the respiratory influence in the HRV.

In general, the results of the simulation study suggest that the best approaches to characterize the RSA strength are P_{TF}, $\mathcal{P}_x$ and CE. These estimates are robust to changes in characteristics of the respiratory segments and to changes in F_s. It is important to highlight that for the other estimates more complex regression models might improve the MSE.

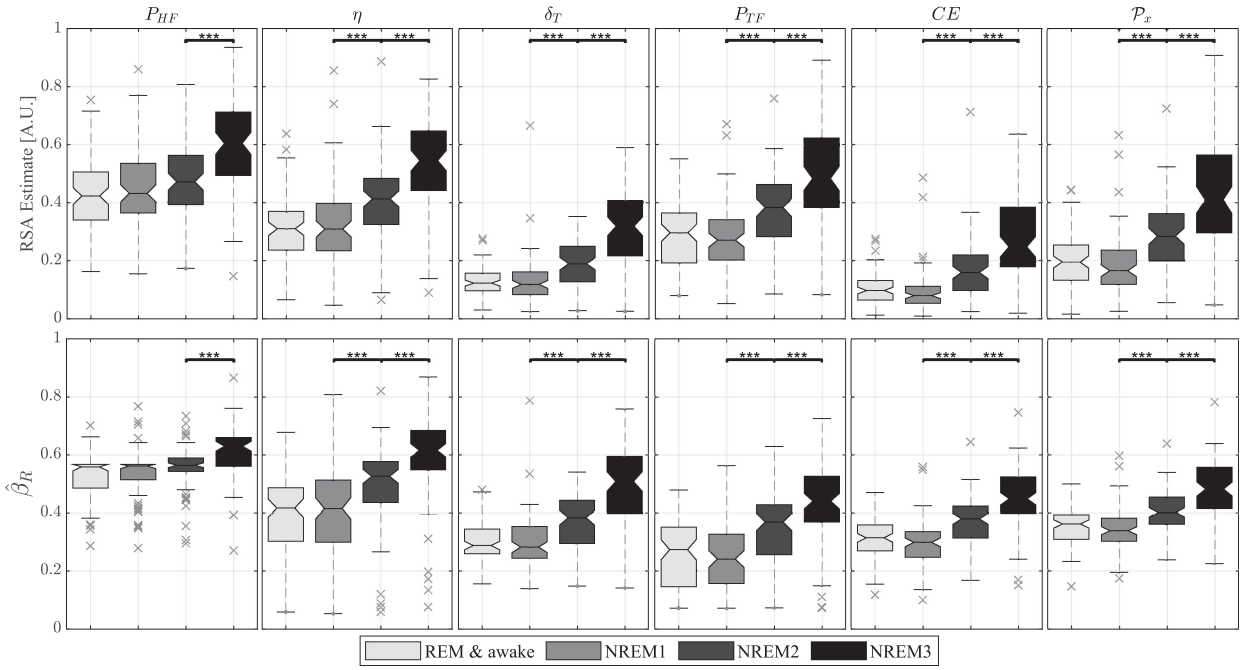

Fig. 9. RSA changes in the sleep dataset. Top row: RSA estimates with the approaches compared in this paper. Each estimate measures the RSA in a different unit and/or scale: $\eta \in [0\ \infty]$ and is given in s^{-1}; $CE \in [0\ \infty]$ and is unit less; P_{HF}, δ_T, P_{TF} and $\mathcal{P}_x \in [0\ 1]$ and are given as ratios, but each of them correlates differently to the RSA. Bottom row: equivalent $\hat{\beta}_R$ for each RSA estimate after using the SVM regression models. $\hat{\beta}_R \in [0\ 1]$ and is the proportion of variance due to the respiratory component in the modulating signal. Significant differences between sleep stages were tested with Friedman's test for repeated measures.

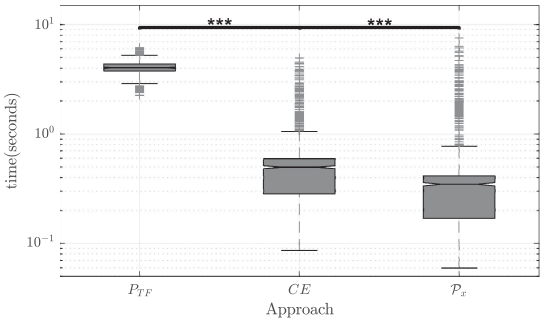

Fig. 10. Execution times for P_{TF}, CE and $\mathcal{P}_x$.

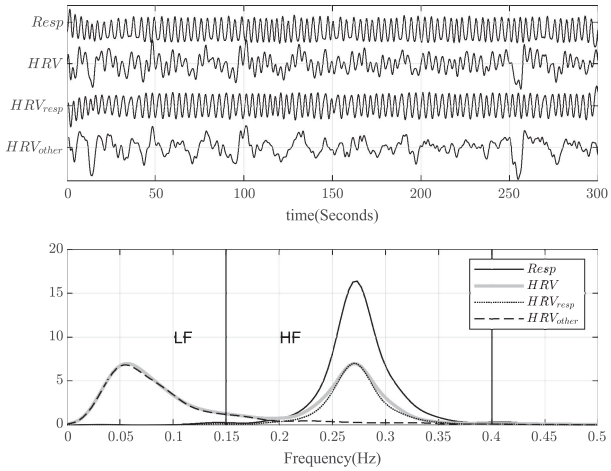

Fig. 11. Example of a respiratory and a HRV epochs taken from the sleep dataset. In this case, $P_{HF} = 0.53$ and $\mathcal{P}_x = 0.41$. Here, the respiratory signal has a narrow bandwidth and falls inside the HF band. The vertical bars show the limits of the standard HF band.

B. Application to Real Data

As expected, the cardiorespiratory coupling is weaker during lighter sleep stages and wake [34], [35]. It is observed that the estimation with $\mathcal{P}_x$ produces smaller values compared to P_{HF} in all sleep stages. This suggests that the weight of modulators other than the respiration was higher compared to the respiratory ones, in accordance with the simulation.

At this point, two previous works can be discussed taking into account the results presented in Section III-B. In [16] and [50], it was shown that P_{HF} underestimates the percentage of power explained by the respiration in the HRV. In both cases, the data was recorded in a controlled environment. In contrast, the work reported in [49] and the results presented in Section III-B indicate that P_{HF} is an overestimation of the cardiorespiratory coupling. According to the results in the simulation, this might indicate that the weight of modulations related to the respiration were stronger in [16] and [50], with a $\beta_R > 0.5$.

Another possible explanation is shown in Fig. 11, which shows an example of the RSA estimation in a 5-minutes epoch taken from the sleep dataset. In this case, P_{HF} resulted in a higher estimation of the cardiorespiratory coupling. This example is different to the results presented in Fig. 5, in which P_{HF}

estimated a smaller value than $\mathcal{P}_x$. When irregular respirations with frequency components below the HF band occur, P_{HF} estimates a weaker RSA strength. On the other hand, when a regular respiratory rate occurs, and this is inside the HF, P_{HF} is higher because it also considers power due to frequency components which $\mathcal{P}_x$ discards.

C. Comments on the Methodology

The methodology to calculate CE, δ_T and $\mathcal{P}_x$ are similar in the sense that they use MVAR models. The difference between them is the way the model is used and interpreted. In the case of CE, the information is estimated as the residual of the regressions between the current samples of the HRV and the past information of the respiration. δ_T uses the same model but it works in the frequency domain to estimate the interaction between the cardiac and respiratory systems. To this end, it quantifies the power contribution of the poles representing different frequency components. $\mathcal{P}_x$ is also an MVAR model in which the current sample in the HRV is a linear combination of the past samples of the HRV, but the coefficients are calculated using the subspace built with the respiratory signal.

The calculation of CE, $\mathcal{P}_x$ and δ_T requires the tuning of L. In this work, this tunning was first tested with AIC and MDL but the results were not always consistent. In some cases, the L selected with the two approaches were too different. In addition, the selection usually resulted in large model orders causing overfitting problems. For these reasons, it was decided to use the empirical approach described in Section II-C2. In addition, the use of a high sampling frequency introduces redundancy in the selection of L. This is particularly problematic for δ_T because the number of poles is related to L, and a higher order than needed will produce poles with negative power [30]. More research on the selection of the model orders might improve the use of the methods to estimate the RSA and is proposed as future work.

Each method can be applied in particular conditions which can occur in cardiorespiratory analysis. P_{HF} is limited to cases in which the respiratory power falls inside the HF band. P_{BW} and η are good options when the respiratory signal is regular with a narrow bandwidth even if it is outside the HF band, but have problems when the respiration has a broad bandwidth or overlap with the peak in the LF. P_{TF} is recommended in cases in which the signals are not stationary. To use δ_T, the HRV and respirations should be resampled to the smallest possible sampling frequency while avoiding aliasing effects and preserving the important information in the HRV and respiration. $\mathcal{P}_x$ and CE are the most robust ones among the compared approaches.

Furthermore, it is important to highlight that the model used in the simulation study assumes β_R to mimic the RSA strength. In addition, the modulations uncorrelated with respiration are simulated with the coefficients of an AR model taken from a healthy subject. The same simulation for a diseased population would require adjustments to consider the disturbance in sympathovagal balance for each condition. Finally, it has been shown that the RSA has a non-linear relationship with the respiratory frequency [51]. A limitation of the model is that it does not consider these non-linearities, therefore, future studies should focus on including them for a complete estimation of the RSA.

V. Conclusion

RSA has been suggested as marker of cardiovascular function and it has been associated with chronic diseases. Despite this, the methods to assess RSA are not standardized and it is difficult to define objective criteria to compare them. The model proposed in this paper offers a framework for this task and contributes to the standardization of the RSA evaluation, leading to a more accurate RSA estimation in clinical practice.

All the results indicate that, among the compared methods, the approaches based on transfer entropy, time frequency coherence and subspace projections are more robust to estimate the cardiorespiratory coupling in simulated as well as in real data.

References

[1] R. P. Bartsch *et al.*, "Three independent forms of cardio-respiratory coupling: Transitions across sleep stages," in *Proc. Comput. Cardiol.*, 2014, pp. 781–784.

[2] G. E. Billman, "Heart rate variability–a historical perspective," *Frontiers Physiol.*, vol. 2, p. 86, 2011.

[3] G. Anrep, W. Pascual, and R. Rössler, "Respiratory variations of the heart rate-I-the reflex mechanism of the respiratory arrhythmia," in *Proc. Roy. Soc. London. Ser. B-Biol. Sci.*, vol. 119, no. 813, 1936, pp. 191–217.

[4] M. Piepoli *et al.*, "Origin of respiratory sinus arrhythmia in conscious humans: An important role for arterial carotid baroreceptors," *Circulation*, vol. 95, no. 7, pp. 1813–1821, 1997.

[5] C. Bainton *et al.*, "Respiratory modulation of sympathetic activity," *J. Auton. Nervous Syst.*, vol. 12, no. 1, pp. 77–90, 1985.

[6] G. G. Berntson, J. T. Cacioppo, and K. S. Quigley, "Respiratory sinus arrhythmia: Autonomic origins, physiological mechanisms, and psychophysiological implications," *Psychophysiology*, vol. 30, no. 2, pp. 183–196, 1993.

[7] J. Hayano *et al.*, "Respiratory sinus arrhythmia: A phenomenon improving pulmonary gas exchange and circulatory efficiency," *Circulation*, vol. 94, no. 4, pp. 842–847, 1996.

[8] P. Y. Sin *et al.*, "Interactions between heart rate variability and pulmonary gas exchange efficiency in humans," *Exp. Physiol.*, vol. 95, no. 7, pp. 788–797, 2010.

[9] A. Ben-Tal, S. S. Shamailov, and J. F. Paton, "Central regulation of heart rate and the appearance of respiratory sinus arrhythmia: New insights from mathematical modeling," *Math. Biosci.*, vol. 255, pp. 71–82, 2014.

[10] M. Elstad, "Respiratory variations in pulmonary and systemic blood flow in healthy humans," *Acta Physiologica*, vol. 205, no. 3, pp. 341–348, 2012.

[11] M. Elstad *et al.*, "Respiratory sinus arrhythmia stabilizes mean arterial blood pressure at high-frequency interval in healthy humans," *Eur. J. Appl. Physiol.*, vol. 115, no. 3, pp. 521–530, 2015.

[12] W. Hrushesky *et al.*, "The respiratory sinus arrhythmia: A measure of cardiac age," *Sci.*, vol. 224, no. 4652, pp. 1001–1004, 1984.

[13] J. Mackay, "Respiratory sinus arrhythmia in diabetic neuropathy," *Diabetologia*, vol. 24, no. 4, pp. 253–256, 1983.

[14] M. R. Bonsignore *et al.*, "Respiratory sinus arrhythmia during obstructive sleep apnoeas in humans," *J. Sleep Res.*, vol. 4, pp. 68–70, 1995.

[15] M. Peltola *et al.*, "Respiratory sinus arrhythmia as a predictor of sudden cardiac death after myocardial infarction," *Ann. Med.*, vol. 40, no. 5, pp. 376–382, 2008.

[16] C. Varon *et al.*, "Unconstrained estimation of HRV indices after removing respiratory influences from heart rate," *IEEE J. Biomed. Health Inform.*, vol. 23, no. 6, pp. 2386-2397, Nov. 2019.

[17] S. M. Gorka *et al.*, "Association between respiratory sinus arrhythmia and reductions in startle responding in three independent samples," *Biol. Psychol.*, vol. 93, no. 2, pp. 334–341, 2013.

[18] L. Sörnmo and P. Laguna, *Bioelectrical Signal Process. Cardiac Neurological Appl.*, New York, NY, USA: Academic Press, 2005, vol. 8.

[19] A. J. Camm *et al.*, "Heart rate variability: Standards of measurement, physiological interpretation and clinical use. task force of the european society of cardiology and the north american society of pacing and electrophysiology," 1996.

[20] T. E. Brown *et al.*, "Important influence of respiration on human RR interval power spectra is largely ignored," *J. Appl. Physiol.*, vol. 75, no. 5, pp. 2310–2317, 1993.
[21] J. Schipke, G. Arnold, and M. Pelzer, "Effect of respiration rate on short-term heart rate variability," *J. Clin. Basic Cardiol.*, vol. 2, no. 1, pp. 92–95, 1999.
[22] E. O'Callaghan *et al.*, "Cardiac output is improved in rats with myocardial infarction by enhancement of respiratory sinus arrhythmia," *The FASEB J.*, vol. 29, no. 1_supplement, pp. 1043–3, 2015.
[23] T. M. Shader *et al.*, "Quantifying respiratory sinus arrhythmia: Effects of misspecifying breathing frequencies across development," *Develop. Psychopathol.*, vol. 30, no. 1, pp. 351–366, 2018.
[24] J. F. Morales Tellez *et al.*, "Evaluation of methods to characterize the change of the respiratory sinus arrhythmia with age in sleep apnea patients," in *Proc. Eng. Med. Biol. Soc.*, 2019, pp. 1588-1591.
[25] M. T. V. Yamuza *et al.*, "Human emotion characterization by heart rate variability analysis guided by respiration," *IEEE J. Biomed. Health Inform.*, vol. 23, no. 6, pp. 2446–2454, Nov. 2019.
[26] R. Bailón *et al.*, "Analysis of heart rate variability using time-varying frequency bands based on respiratory frequency," in *Proc. 29th Annu. Int. Conf. IEEE Eng. Med. Biol. Soc.*, 2007, pp. 6674–6677.
[27] M. Orini *et al.*, "Characterization of dynamic interactions between cardiovascular signals by time-frequency coherence," *IEEE Trans. Biomed. Eng.*, vol. 59, no. 3, pp. 663–673, Mar. 2012.
[28] R. Joshi *et al.*, "Cardiorespiratory coupling in preterm infants," *J. Appl. Physiol.*, vol. 126, no. 1, pp. 202–213, 2018.
[29] S. Nemati *et al.*, "Respiration and heart rate complexity: Effects of age and gender assessed by band-limited transfer entropy," *Respiratory Physiol. Neurobiol.*, vol. 189, no. 1, pp. 27–33, 2013.
[30] L. Faes *et al.*, "A new frequency domain measure of causality based on partial spectral decomposition of autoregressive processes and its application to cardiovascular interactions," in *Proc. 41st Annu. Int. Conf. IEEE Eng. Med. Biol. Soc.*, 2019, pp. 4258–4261.
[31] L. Faes, A. Porta, and G. Nollo, "Information decomposition in bivariate systems: Theory and application to cardiorespiratory dynamics," *Entropy*, vol. 17, no. 1, pp. 277–303, 2015.
[32] R. Bailón *et al.*, "Analysis of heart rate variability during exercise stress testing using respiratory information," *Biomed. Signal Process. Control*, vol. 5, no. 4, pp. 299–310, 2010.
[33] M. Orini *et al.*, "Synthesis of HRV signals characterized by predetermined time-frequency structure by means of time-varying ARMA models," *Biomed. Signal Process. Control*, vol. 7, no. 2, pp. 141–150, 2012.
[34] T. Penzel *et al.*, "Modulations of heart rate, ECG, and cardio-respiratory coupling observed in polysomnography," *Frontiers Physiol.*, vol. 7, p. 460, 2016.
[35] R. P. Bartsch *et al.*, "Phase transitions in physiologic coupling," in *Proc. Nat. Acad. Sci.*, vol. 109, pp. 10181–10186, 2012.
[36] R. B. Berry *et al.*, "Rules for scoring respiratory events in sleep: Update of the 2007 AASM manual for the scoring of sleep and associated events," *J. Clin. Sleep Med.*, vol. 8, no. 05.
[37] J. Healey *et al.*, "Detecting stress during real-world driving tasks using physiological sensors," *IEEE Trans. Intell. Transp. Syst.*, vol. 6, no. 2, pp. 156–166, Jun. 2005.
[38] N. Iyengar *et al.*, "Age-related alterations in the fractal scaling of cardiac interbeat interval dynamics," *Amer. J. Physiol.-Regulatory, Integrative Comparative Physiol.*, vol. 271, no. 4, pp. R1078–R1084, 1996.
[39] J. Mateo and P. Laguna, "Improved heart rate variability signal analysis from the beat occurrence times according to the IPFM model," *IEEE Trans. Biomed. Eng.*, vol. 47, no. 8, pp. 985–996, Aug. 2000.
[40] A. Malliani *et al.*, "Cardiovascular neural regulation explored in the frequency domain," *Circulation*, vol. 84, no. 2, pp. 482–492, 1991.
[41] M. Pagani *et al.*, "Power spectral analysis of heart rate and arterial pressure variabilities as a marker of sympatho-vagal interaction in man and conscious dog," *Circulation Res.*, vol. 59, no. 2, pp. 178–193, 1986.
[42] B. Pomeranz *et al.*, "Assessment of autonomic function in humans by heart rate spectral analysis," *Amer. J. Physiol.-Heart Circulatory Physiol.*, vol. 248, no. 1, pp. H151–H153, 1985.
[43] C. Varon *et al.*, "A novel algorithm for the automatic detection of sleep apnea from single-lead ECG," *IEEE Trans. Biomed. Eng.*, vol. 62, no. 9, pp. 2269–2278, Sep. 2015.
[44] R. Bailón *et al.*, "The integral pulse frequency modulation model with time-varying threshold: Application to heart rate variability analysis during exercise stress testing," *IEEE Trans. Biomed. Eng.*, vol. 58, no. 3, pp. 642–652, Mar. 2010.
[45] A. Y. Schumann *et al.*, "Bivariate phase-rectified signal averaging," *Physica A: Statist. Mech. Appl.*, vol. 387, no. 21, pp. 5091–5100, 2008.
[46] M. Orini *et al.*, "A time-varying nonparametric methodology for assessing changes in QT variability unrelated to heart rate variability," *IEEE Trans. Biomed. Eng.*, vol. 65, no. 7, pp. 1443–1451, Jul. 2017.
[47] L. Faes, G. Nollo, and A. Porta, "Information decomposition: A tool to dissect cardiovascular and cardiorespiratory complexity," in *Proc. Complexity Nonlinearity Cardiovascular Signals*, Springer, 2017, pp. 87–113.
[48] A. Montalto, L. Faes, and D. Marinazzo, "MuTE: A MATLAB toolbox to compare established and novel estimators of the multivariate transfer entropy," *PloS One*, vol. 9, no. 10, 2014.
[49] J. F. Morales Tellez *et al.*, "Evaluation of methods to characterize the change of the respiratory sinus arrhythmia with age in sleep apnea patients," in *Proc. IEEE Eng. Med. Biol. Soc.*, 2019, pp. 1588-1591.
[50] J. Morales *et al.*, "Effect of the heart rate variability representations on the quantification of the cardiorespiratory interactions during autonomic nervous system blockade," in *Proc. Comput. Cardiol.*, 2019, pp. Page 1–Page 4.
[51] A. Angelone and N. A. Coulter JR, "Respiratory sinus arrhythmia: A frequency dependent phenomenon," *J. Appl. Physiol.*, vol. 19, no. 3, pp. 479–482, 1964.